Finite Element Analysis of an External Fixator with Composite Connecting Rods

E. V. Caburnay, L. M. Danao. E. D. Magdaluyo Jr.

***Abstract*— This study aims to analyze the performance of an external fixator model using a combination of finite element analysis and composite layering software. A 3D CAD model of the external fixator was developed, and the relevant materials and their properties were assigned to different parts of the model. Stress and deformation analyses were then conducted by subjecting the external fixator to axial compression, torsion, and bending loads. The simulation results showed that the 18 mm woven carbon fiber-epoxy composite rod outperformed the 12 mm stainless steel rod during axial compression. The pin diameter was increased to 6 mm, which reduced the stresses in the critical areas below the yield strength of the material. Overall, this study contributes to the advancement of external fixator modeling and finite element analysis, as well as highlights the potential of composite materials in improving the performance of external fixators.**

***Index Terms*—Finite Element Analysis, External Fixators, Tibial Fractures, Composite Materials**

I. Introduction

Tibial fractures are common results of high-energy trauma such as vehicular accidents, sports activities, and workplace related injuries [1-4]. External fixation is a widely used treatment method for tibia fractures when soft tissue management is necessary [5]. Compared to other treatments, the process of external fixation is less invasive and induces less swelling [6-7]. The external fixator serves as an external scaffold attached to the bone to stabilize the fractured bone during the healing process. This is especially important for the long bones located in the lower extremities, which carry a significant amount of the body's weight. Pins or wires are used to secure the external fixator to the bone.

Various experimental and simulation studies have been conducted to assess the performance of the external fixators under different loading conditions and to facilitate the design or redesign of these biomedical devices. Retrospective studies have been carried out to analyze the data from past patients who were treated with external fixators [8-9]. The use of finite element analysis (FEA) software has been beneficial in evaluating the stresses, deformations, and strains of external fixators without the need for physical prototypes. In some cases, the bone models generated from computerized tomography (CT) scans have been utilized [10-11], while in others, simplified bone models have been used [12-13]. The FEA has been applied to determine the stiffness and stress distribution in both the external fixator and the bone [14-15].

There has been a growing trend towards the use of fiber-reinforced polymers (FRPs) in the fabrication of external fixators. These materials consist of two or more constituent materials with differing chemical or physical properties and have a lower density while still maintaining high material strength compared to conventional external fixator materials such as the stainless steel [16]. Although previous research has utilized FEA and composite layering software to analyze the rod of an external fixator, there are limited studies performed on the use of carbon fiber-epoxy rods created using the composite layering software in an external fixator model. Thus, this study aims to address the gap by designing and analyzing an external fixator, creating composite rods with properly oriented fibers using the composite layering software, and comparing their performance to that of a commonly used stainless-steel rod.

II. Methodology

Fig. 1a shows the model used for the simulations in this study. The external fixator frame was designed using 3D CAD software, and the model includes four clamps attached to a single connecting rod. Each clamp is connected to a pin, which in turn is attached to a fragment of the bone model with a fracture gap. The clamps of the external fixator frame were based on the *Depuy Synthes* modular external fixator, chosen for its modularity and flexibility during half pin application to the bone [17]. The design was modified to allow the clamps to attach to two half pins. As shown in Fig. 1b, the outer diameter of the bone model, fracture gap, bone fragment length, and the diameter and length of the connecting rod were 38 mm, 10 mm, 180 mm, 12 mm, and 300 mm, respectively. The thickness of the cortical section of the simplified bone is 7.125 mm, while the diameter of the cancellous section is 23.75 mm [18].

Table 1 summarizes the material properties utilized in FEA simulations using ANSYS Workbench 2021 R1. The bone model consists of a cortical bone in the outer section, and cancellous bone in the inner section. Stainless steel 304 was assigned to the pins and nuts, while the 7075 T6 Aluminum was assigned to the other parts of the clamp. The connecting rod was fabricated using two types of composite fiber reinforced polymers: Unidirectional (UD) Epoxy Carbon (230 GPa) prepreg and Woven Epoxy Carbon (230 GPa) prepreg. The different properties being used in the simulation are already embedded in the FEA software. Table 2 shows the composite material properties used in the simulations.

Manuscript received March 25, 2023; revised June 31, 2023.

This research was funded by the Department of Science and Technology – Philippine Council for Health Research and Development.

E. V. Caburnay is a Science Research Specialist II of the University of the Philippines Surgical Innovations and Biotechnology Laboratory (phone: +63906-221-7344; e-mail: epcaburnay@gmail.com).

L. M. Danao is a professor of the University of the Philippines Diliman Department of Mechanical Engineering (e-mail: louisdanao@up.edu.ph).

E. D. Magdaluyo, Jr. is a Associate Professor of the University of the Philippines Diliman Department of Mining, Metallurgical and Materials Engineering. (e-mail: edmagdaluyo1@up.edu.ph).

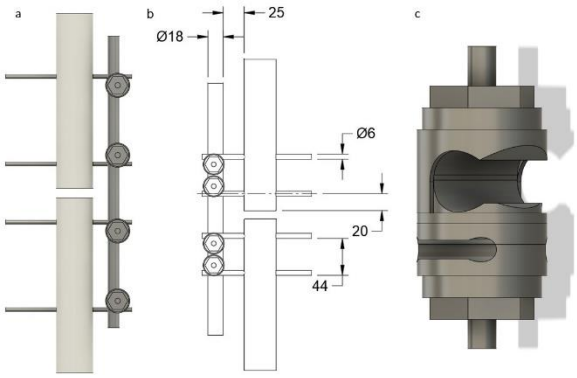

Fig. 1: (a) 3D Model of the external fixator frame connected to the bone, (b) external fixator model dimensions (mm), and (c) closeup of the clamp design

Table 1: Material properties used for finite element analysis

Property	Cortical Bone	Cancellous Bone	304 SS	7075 T6 Al	Epoxy Carbon UD	Epoxy Carbon Woven
E1 (GPa)					121	61.34
E2 (GPa)	7.3	1.1	193	71.7	8.6	61.34
E3 (GPa)					8.6	6.9
G12 (GPa)					4.7	3.3
G23 (GPa)	-	-	-	-	3.1	2.7
G13 (GPa)					4.7	2.7
v12					0.27	0.04
v23	0.3	0.26	0.29	0.33	0.4	0.3
v13					0.27	0.3
TS (MPa)	71.56	4.4	215	503	-	-
Tangent Modulus (GPa)	-	-	1.8	0.5	-	-

Table 2: Stress and strain limits of built-in composite materials used

Property	Epoxy Carbon UD Prepreg		Epoxy Carbon Woven Prepreg	
	Stress (MPa)	Strain (mm/mm)	Stress (MPa)	Strain (mm/mm)
Tensile 1	2231	0.0167	805	0.0126
Tensile 2	29	0.0032	805	0.0126
Tensile 3	29	0.0032	50	0.008
Compressive 1	-1082	-0.0108	-509	-0.0102
Compressive 2	-100	-0.0192	-509	-0.0102
Compressive 3	-100	-0.0192	-170	-0.012
Shear 12	60	0.12	125	0.022
Shear 23	32	0.11	65	0.019
Shear 13	60	0.12	65	0.019

The simulation process involved isolating first the connecting rod since fiber reinforced polymer composite material was assigned. The other parts were suppressed using the CAD module embedded in the FEA software. The composite layering module was utilized to set the thickness of the shell of the connecting rod model to 1 mm, and to properly orient the fibers of the connecting rod. The ply thickness was specified to be 0.18 mm [19] and the number of layers were specified to model a solid composite rod. The orientation of the fibers was set along the longitudinal axis of the rod and another with fibers oriented in -45, 0, 45, 0 angles to investigate the effect of angled fiber orientations on the maximum deformation results of the external fixator model. The performance of the composite rods was compared to the performance of the 12 mm stainless steel rod. Size increases were conducted to the diameter of the composite rod until the external fixator model with the composite rod outperformed the external fixator model with the stainless steel rod.

Fig. 2a-c illustrates the loading conditions applied to the external fixator model. A compressive axial load was applied to the proximal end with a magnitude of 350 N [4]. This value was derived from 50% of the weight of a person weighing 700 N, since 50% of the weight is experienced during stance phase. A torsional load of 6.75 Nm was also applied on the same location, while a 500 N of bending load was applied at the pins closer to the fracture gap [19]. It is important to note that the load magnitudes used in this study were only utilized to analyze the performance of the external fixator model, as full weight bearing is not recommended for unilateral external fixators. The distal end was fixed for the compressive axial and torsional loads, while zero-displacement supports were placed on a vertex on both the proximal and distal ends. On the other hand, large deflections were turned on in the software for the stainless-steel rod analysis to account for the nonlinear regions of the stress-strain curves of the materials. Fig. 2d shows the modules of the external fixator frame and the connecting rod with properly oriented fibers combined in a static structural block in the FEA software workbench. After setting all the parameters and constraints in the FEA software, the stress and deformation analyses were performed to determine the response of the external fixator model to the different loading conditions.

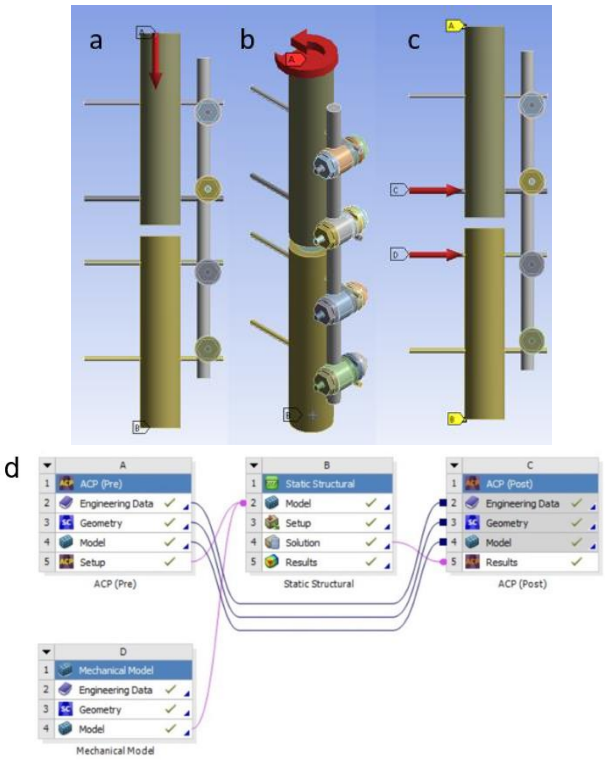

Fig. 2: (a) compression, (b) torsion, and (c) bending loads, (d) modules connected in the FEA software

III. Results and Discussion

In order to validate the simulation process from this study, a comparison was made between the simulation and experimental data from previous study [17]. The results showed an error of 9.90% and 6.29% at 300 N and 400 N, respectively, indicating that the simulations slightly

ISBN: 978-988-14049-4-7
ISSN: 2078-0958 (Print); ISSN: 2078-0966 (Online)

overpredicted the maximum deformation compared to the experimental values. To further ensure the accuracy of the simulations, a mesh refinement study was also performed using two different mesh size, 3 mm and 1.5 mm element size. Both meshes were subjected to fast transition, coarse span angle center, and medium smoothing. The maximum deformation results showed only a 0.69% difference between the two meshes, and hence, the mesh with 3 mm element size was used for all analyses.

The composite rod of the external fixator shown in Fig. 1a was compared to the same external fixator model utilizing a 304 stainless steel rod. Both rods had an initial diameter of 12 mm, which is within the range of commonly available rod diameters of 8 mm to 14 mm and is also the diameter used by the *Depuy Synthes* modular external fixator [20]. Unidirectional Carbon Fiber-Epoxy (Prepreg) embedded in the finite element analysis software was used as the material of the composite rod.

Fig. 3 shows the maximum equivalent von-Mises stresses resulting from the three loading conditions of axial compression, torsion and bending. The external fixator model with a stainless-steel rod exhibited maximum total deformations of 1.7028 mm, 3.359 mm, and 1.7724 mm for the applied loads, respectively. However, increasing the diameter of the pins from 4.7 mm to 6 mm reduced the maximum deformation experienced by the external fixator. The maximum deformation values for all loading conditions decreased to 1.4494 mm, 1.4546 mm, and 1.1108 mm for the external fixator model with 6 mm pins. In analyzing the maximum equivalent von-Mises stress shown in Fig. 3a-3c, it is apparent that the highest stresses, with values of 254.57 MPa, 258.44 MPa, and 312.65 MPa, occur where the pin and the pin clamp are connected. The stress values exceed the yield strength of 304 stainless steel, which is 215 MPa. This is due to the sharp edges present in the pin clamp and bone outermost parts, creating stress concentrations in the pins, pin clamps, and bone. It is important to note that the limitation of this study, where all contact regions are perfectly bonded, causes higher stresses to occur at contact regions due to the connected parts' inability to slide or separate [21].

When the equivalent von Mises stress exceeds the material's yield strength, ductile materials will yield [22]. Therefore, one way to alleviate stress concentration in this area is to add fillets to round out the sharp edge. Increasing the pin diameter to 6 mm also reduced the maximum von Mises stresses experienced by the pins as shown in Fig. 3d.

The composite rod was set to have 28 layers, which is the maximum number of layers that can be used without encountering an error for the 12 mm composite rod. Table 3 shows that the 12 mm unidirectional carbon fiber-epoxy composite rod experienced higher deformation in all loads when compared to the 12 mm stainless steel rod. Specifically, the external fixator model with the 12 mm unidirectional composite rod experienced maximum deformation results of 2.8911 mm, 4.1269 mm, and 2.0999 mm, which translated to 84.13% higher deformation in axial compression, 116.66% higher deformation in torsion, and 79.16% higher deformation in bending loads compared to the external fixator model with 12 mm stainless steel rod. To decrease the deformation experienced by the model below that of the 12 mm stainless steel rod, the diameter of the composite rod was increased to 14 mm. Increasing the radius of the rod results in an increase in the stiffness of the external fixator model [20]. The 14 mm diameter was selected since this was the maximum rod size usually offered by manufacturers [22]. The increase in diameter size had a positive effect in decreasing the deformation experienced by the external fixator, but it was not enough to outperform the 12 mm stainless steel rod. The deformation results of the 14 mm unidirectional rod are 2.0299 mm, 3.8568 mm, and 1.6359 mm, which are larger by 29.28%, 102.478%, and 39.57% than the maximum deformation results of the 12 mm stainless steel rod for axial compression, torsion, and bending loads, respectively. The response of the composite materials to the axial compression, torsion and bending with further increased diameter rod is also shown in Table 3.

The unidirectional rod was also analyzed for composite failure using Tsai-Wu criterion [23] Fig. 4a shows that the rod fails at multiple elements for torsion with a minimum factor of safety value of 0.41477. The failure areas are located where the clamps are attached. On the other hand, no failure occurs for axial compression and bending loading, with minimum factor of safety values of 11.363 and 3.8, respectively.

Using the Maximum Stress criterion, the unidirectional rod fails under torsion or bending loads. As seen in Fig. 4b, under torsion, the minimum factor of safety value of 0.4116 and the failed elements indicate s2t, which means matrix failure due to tension. The next layer also experienced failure, with a minimum factor of safety value of 0.9623. The unidirectional composite rod did not experience composite failure during axial compression or bending loads.

Since the unidirectional composite rod failed under torsion loading, woven carbon fiber epoxy composite rods were also modelled and compared to the performance of the 12 mm 304 stainless steel. Table 3 shows that the 16 mm woven composite rod performed worse compared to the unidirectional composite rod. This is due to the lower elastic modulus provided by the embedded woven carbon fiber epoxy embedded in the software. The deformation experienced by the 16 mm woven composite rod when loaded with axial compression, with total deformation value of 1.9772 mm, was 25.928% higher than the deformation experienced by the 12 mm stainless steel rod, while the deformation it experienced during torsion, with a value of 3.1574 mm, was 65.76% higher. Similarly, the deformation value during the bending load of 1.6197 mm was 38.188% higher than the deformation experienced by the 12 mm stainless steel rod.

The stresses and strains in the composite rods were also analyzed. The maximum and minimum strains were obtained for each of the rods, and different composite failure criteria were utilized to check for failure on the composite rods. Utilizing both the Tsai-Wu and Maximum Stress criteria, no failure was observed on the 16 mm woven composite rod. To further investigate the performance of the woven composite rod, its diameter was increased to 18 mm. This decreased the difference in deformation between the 18 mm woven composite rod and the 12 mm stainless steel rod to 2.76%, as the maximum deformation result for the 18 mm was 1.5267 mm under axial compression, and 1.3945 mm under bending load, which was a difference of 18.974% compared to the 12 mm stainless steel rod. For the torsion load, the 18 mm rod

ISBN: 978-988-14049-4-7
ISSN: 2078-0958 (Print); ISSN: 2078-0966 (Online)

returned a maximum deformation result of 3.1225 mm, which was a difference of 63.927% compared to the 12 mm stainless steel rod. As a result, the 18 mm woven composite rod was able to outperform the 12 mm stainless steel rod with 6 mm pins.

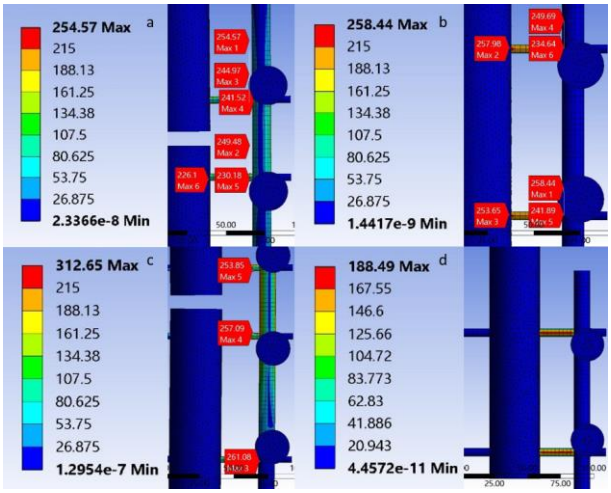

Fig. 3: Maximum equivalent von-Mises stresses caused by (a) axial compression, (b) torsion, and (c) bending loads on the external fixator with stainless steel rod, (d) locations of maximum von Mises stress for the external fixator with 6 mm pins loaded in torsion

Table 3: Comparison the maximum deformation of different rod materials at varying rod diameter

Rod material	Rod diameter	Maximum deformation (mm)		
		Axial compression	Torsion	Bending
304 stainless steel	12 mm	1.5701	1.9048	1.1721
CF-Epoxy UD	12 mm	2.8911	4.1269	2.0999
CF-Epoxy UD	14 mm	2.0299	3.8568	1.6359
CF-Epoxy UD	15 mm	1.5282	3.5243	1.414
CF-Epoxy UD	16 mm	1.2427	2.9462	1.2605
CF-Epoxy woven	16 mm	1.9772	3.1574	1.6197
CF-Epoxy woven	18 mm	1.5267	3.1225	1.3945

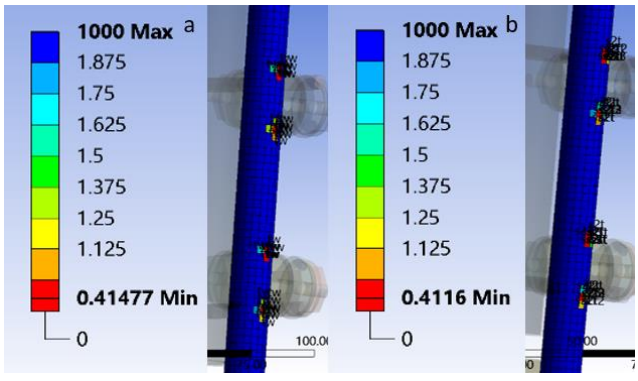

Fig. 4: Failure of the unidirectional composite rod under the (a) Tsai-Wu criterion and (b) Maximum stress criterion

The use of a woven carbon fiber-epoxy rod is better over the unidirectional rod for the external fixator, as none of its layers experience failure in any loading condition according to both the Tsai-Wu criterion and the Maximum Stress criterion. Although the woven carbon fiber-epoxy rod experienced higher deformation during axial compression loads, it is still better compared to the unidirectional rod. However, since the external fixator experiences a combination of loads [24], it is difficult to use the unidirectional composite rod due to its failure in torsional and bending loading. Increasing the diameter of the woven composite rod can be a solution to reduce the deformation experienced by the external fixator.

IV. Conclusion

An external fixator model for tibial fracture with composite connecting rods was analyzed after being subjected to axial compressive, torsion, and bending loads. The recommended ideal external fixator configuration includes a pin diameter of 6 mm and a woven composite rod diameter of 18 mm. This model showed higher stiffness during axial compression compared to the 12 mm stainless steel rod and 16 mm unidirectional composite rod, while not experiencing any composite failure in any of its layers.

Acknowledgment

The authors would like to extend special thanks to the Capacity-building and Incubation Program: Establishment of the University of the Philippines Manila (UPM) College of Medicine (UPCM) – Philippine General Hospital (PGH) Surgical Innovation and Biotechnology Laboratory (SIBOL) for this project, as well as the Engineering Research and Development for Technology of the Department of Science and Technology.

References

[1] Kapukaya, A., Subasi, M., Arslan, H., & Tuzuner, T. (2005). Non-reducible, open tibial plafond fractures treated with a circular external fixator (is the current classification sufficient for identifying fractures in this area?). Injury, 36(12), 1480–1487. https://doi.org/10.1016/j.injury.2005.05.005

[2] Lawal, Y. Z., Ejagwulu, F. S., Salami, S. O., & Mohammed, S. (2016). Monolateral frame external fixators in the definitive management of open limb fractures in north-western Nigeria. Sub-Saharan African Journal of Medicine, 3(3), 137. https://doi.org/10.4103/2384-5147.190847

[3] Piper, K. J., Won, H. Y., & Ellis, A. M. (2005). Hybrid external fixation in complex tibial plateau and plafond fractures: An Australian audit of outcomes. Injury, 36(1), 178–184. https://doi.org/10.1016/j.injury.2004.04.006

[4] Ramlee, M., Abdul Kadir, M., Murali, M., & Kamarul, T. (2014). Finite element analysis of three commonly used external fixation devices for treating Type III pilon fractures. Medical Engineering & Physics, 36(10), 1322-1330. doi: 10.1016/j.medengphy.2014.05.015

[5] Fragomen, A., & Rozbruch, S. (2006). The Mechanics of External Fixation. HSS Journal, 3(1), 13-29. doi: 10.1007/s11420-006-9025-0

[6] Claes, L., Heitemeyer, U., Krischak, G., Braun, H., & Hierholzer, G. (1999). Fixation technique influences osteogenesis of comminuted fractures. Clinical Orthopaedics and Related Research, 365, 221–229. https://doi.org/10.1097/00003086-199908000-00027

[7] Kouassi, K., Cartiaux, O., Fonkoué, L., Detrembleur, C., & Cornu, O. (2020). Biomechanical study of a low-cost external fixator for diaphyseal fractures of long bones. Journal Of Orthopaedic Surgery and Research, 15(1). doi: 10.1186/s13018-020-01777-5

[8] Bove, F., Sala, F., Capitani, P., Thabet, A., Scita, V., & Spagnolo, R. (2018). Treatment of fractures of the tibial plateau (Schatzker VI) with external fixators versus plate osteosynthesis. Injury, 49, S12-S18. doi: 10.1016/j.injury.2018.09.059

[9] Hadeed, M., Evans, C., Werner, B., Novicoff, W., & Weiss, D. (2019). Does external fixator pin site distance from definitive implant affect infection rate in pilon fractures?. Injury, 50(2), 503-507. doi: 10.1016/j.injury.2018.10.041

[10] Abd Aziz, A., Abdul Wahab, A., Abdul Rahim, R., Abdul Kadir, M., & Ramlee, M. (2020). A finite element study: Finding the best

configuration between unilateral, hybrid, and ilizarov in terms of biomechanical point of view. Injury, 51(11), 2474-2478. doi: 10.1016/j.injury.2020.08.001

[11] Liang, B., Chen, Q., Liu, S., Chen, S., Yao, Q., & Wei, B. et al. (2020). A feasibility study of individual 3D-printed navigation template for the deep external fixator pin position on the iliac crest. BMC Musculoskeletal Disorders, 21(1). doi: 10.1186/s12891-020-03509-6

[12] Kolasangiani, R., Mohandes, Y., & Tahani, M. (2020). Bone fracture healing under external fixator: Investigating impacts of several design parameters using Taguchi and ANOVA. Biocybernetics And Biomedical Engineering, 40(4), 1525-1534. doi: 10.1016/j.bbe.2020.09.007

[13] Kolasangiani, R., Parchami, K., & Tahani, M. (2021). Optimization of Connecting Rod Design Parameters for External Fixation System: A Biomechanical Study. The Journal Of Foot And Ankle Surgery. doi: 10.1053/j.jfas.2021.02.01

[14] Elmedin, M., Vahid, A., Nedim, P., & Nedžad, R. (2015). Finite Element Analysis and Experimental Testing of Stiffness of the Sarafix External Fixator. Procedia Engineering, 100, 1598-1607. doi: 10.1016/j.proeng.2015.01.533

[15] Frydrýšek, K., Jořenek, J., Učeň, O., Kub'n, T., Žilka, L., & Pleva, L. (2012). Design of External Fixators used in Traumatology and Orthopaedics – Treatment of Fractures of Pelvis and its Acetabulum. Procedia Engineering, 48, 164-173. doi: 10.1016/j.proeng.2012.09.501

[16] Abdul Wahab, A., Wui, N., Abdul Kadir, M., & Ramlee, M. (2020). Biomechanical evaluation of three different configurations of external fixators for treating distal third tibia fracture: Finite element analysis in axial, bending and torsion load. Computers In Biology And Medicine, 127, 104062. doi: 10.1016/j.compbiomed.2020.104062

[17] Landaeta, F., Shiozawa, J., Erdman, A., & Piazza, C. (2020). Low cost 3D printed clamps for external fixator for developing countries: a biomechanical study. 3D Printing In Medicine, 6(1). doi: 10.1186/s41205-020-00084-3

[18] Maeda, K., Mochizuki, T., Kobayashi, K., Tanifuji, O., Someya, K., & Hokari, S. et al. (2020). Cortical thickness of the tibial diaphysis reveals age- and sex-related characteristics between non-obese healthy young and elderly subjects depending on the tibial regions. Journal Of Experimental Orthopaedics, 7(1). doi: 10.1186/s40634-020-00297-9

[19] Alexander, P., Gonzalo Fdo, C., Arlex, L. and Jose Jaime, G., 2018. Finite element models of carbon fiber reinforced rails for bone transport fixators. 2018 IX International Seminar of Biomedical Engineering (SIB).

[20] Narayan, B. and Giotakis, N., 2007. Stability with unilateral external fixation in the tibia. Strategies in Trauma and Limb Reconstruction, 2(1), pp.13-20.

[21] Courses.ansys.com. 2020. Introduction to Contact. [online] Available at: <https://courses.ansys.com/wp-content/uploads/2019/05/2.5.1-Introduction-on-contact_New_Template_Master.pdf> [Accessed 14 August 2022].

[22] Budynas, R., Nisbett, J. and Shigley, J., 2008. Shigley's mechanical engineering design. 9th ed. New York: McGraw-Hill, p.101.

[23] De Luca, A. and Caputo, F., 2017. A review on analytical failure criteria for composite materials. AIMS Materials Science, 4(5), pp.1165-1185.

[24] Claes, L. and Cunningham, J., 2009. Monitoring the Mechanical Properties of Healing Bone. Clinical Orthopaedics Related Research, 467(8), pp.1964-1971.

ISBN: 978-988-14049-4-7
ISSN: 2078-0958 (Print); ISSN: 2078-0966 (Online)